Chapter 2
Developments in Field Emission Gun Technologies and Advanced Detection Systems

2.1 Cold-Field Emission Technology

To improve image or analysis quality a large signal-to-noise ratio (SNR) is necessary for imaging and spectroscopic techniques to provide high quality and precise measurements. However, the probe current increases as the square of the beam diameter (Reimer 1998). Therefore, combining high spatial resolution with low detection limits in spectroscopic techniques has always been a heartbreak, choosing between imaging resolution or high count rates. Among the kind of SEMs gun technologies, cold-field emission is the one providing the highest gun brightness while reducing significantly the chromatic aberration. Thus, the CFE gun provides a large probe current in a small probe size and tends to conciliate, to a certain extent, the imaging and analysis SEM conditions. However, inside the gun chamber the cold-field emitter attracts contaminants even if high vacuum is used and needs to be cleaned with a daily flashing procedure. The intense flash then results in instability at the surface of the emitter which in turn results in beam instability and "tip noise" during the formation of a very thin but uniform oxide layer at its surface. This instable regime usually begins after a few tens of minutes of high stable emission and lasts at least one or two hours, depending on the systems. This have dramatically limited the practical use of CFE-SEMs in x-ray microanalysis and orientation mapping via EBSD, although after the unstable regime, the system may be stable for several hours but with a significant reduction of the operational beam current.

Recently, carbon nano-tips have been demonstrated as an interesting route for electron extraction from the emitter and higher stability and brightness were reported (Houdellier et al. 2015). However, no commercial instrument using carbon nano-tips is currently available. The last generation of Hitachi CFE guns were fitted with non-evaporative getter (NEG) pumps that permits to obtain a vacuum one order of magnitude lower than the previous generation of CFE guns (Kasuya et al. 2014). Additionally, an auto-flash system is used to clean the emitter by applying a short mild flash after a short period of time, typically a few tens of minutes.

© The Author(s) 2018

N. Brodusch et al., *Field Emission Scanning Electron Microscopy*, SpringerBriefs in Applied Sciences and Technology, https://doi.org/10.1007/978-981-10-4433-5_2

This ensures to benefit from the highest brightness at all time and thus improve, through the brightness term, the beam diameter/probe current relation, as described by Eq. 2.28 in Reimer's (Reimer 1998).

Typical probe current curves, measured with a Faraday cup at the surface plane of the specimen, are plotted in Fig. 2.1 for CFE guns with normal flashing (SU-8000, set 1 and 2) and for an auto-flash system (SU-8230). To facilitate the comparison, the three curves were normalized with the probe current at t = 0 s. The measurements were recorded with E_0 = 30 kV with all column parameters being equal for the three sets of measurements. Each point corresponds to the average of sixty measurement in one second. The curve for SU-8230 was obtained with mild flashes automatically controlled every 65 min. For the SU-8000 SEM, two sets of data were acquired: For set 1, the emission current was reset every 30 min (which increase the extraction voltage of the gun) while set 2 is the observed current after a normal flash without resetting of the emission current. Note that the data shown in set 1 correspond to the normal operation of the typical CFE-SEM. In fact, as deduced from the curve of set 2, the emission current drops dramatically after approximately 30 min with a loss of current of 50% in 1 h. However, when the emission current is reset during this sudden drop, the emission loss is kept below 30% but the unstable regime duration cannot be decreased. It has to be noted that the normal operation procedure is to flash the emitter a few hours before the SEM is being used in order to prevent from the unstable regime during the SEM operation. Following this procedure, the SEM can be operated 5–6 h with an appreciable beam current stability of approximately 3% during this period (Fig. 2.1). As one can see, the auto-flash assisted-CFE gun do not show the dramatic loss of emission observed with the normal flash operation and the working probe current achievable is higher

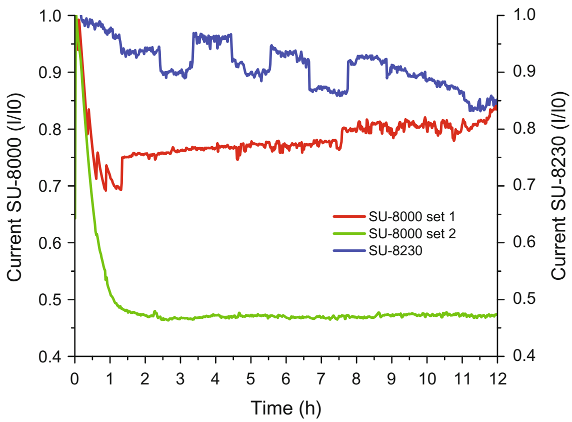

Fig. 2.1 Comparison of normalized electron probe current measured with a Faraday cup at E_0 = 30 kV at the specimen plane for SU-8000 and SU-8230. The same condenser and current parameters were kept identical in all three measurements. Each point is the average of 60 points of 1 s each. For SU-8000 curves, set 1 was obtained with resetting the emission current (I_e) every 30 min while set 2 was obtained without resetting I_e

in average. The current stability is high between each mild flash. However, unexpected emission jumps at mild flashing time are observed and are, to this day, unexplained. Despite the fact that the emission loss is of the order of 15% in 12 h, a higher beam current is achieved with the auto-flash system. This definitely greatly improves the capacity of this type of CFE-SEM to perform x-ray and EBSD analysis in a similar manner to the Schottky FE-SEMs on long periods of time while it was restricted to a few hours with the previous technology of CFE-SEM.

The combination of the reduction of the chromatic aberration due to the low energy spread of the CFE gun and the improvement of the in-lens detection led to a constant improvement of the image quality and resolution as demonstrated in Fig. 2.2. In this figure, SE images are shown from etched Nb(CN) precipitates in steel at an accelerating voltage (E_0) of 5 kV with the Hitachi S-4500 (a), from carbon nanotubes decorated with copper nanoparticles with the Hitachi S-4700 at E_0 = 3 kV (b) and from a lithium titanate powder at E_0 = 2 kV with the Hitachi

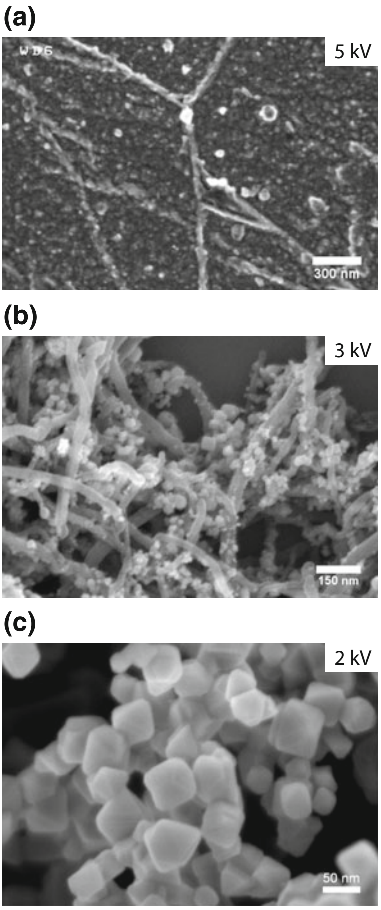

Fig. 2.2 Evolution of the imaging capabilities of the CFE-SEMs through the last 30 years. **a** Hitachi S-4500 at E_0 = 5 kV, **b** Hitachi S-4700 at E_0 = 3 kV and **c** Hitachi SU-8230 at E_0 = 2 kV, high-resolution micrographs

SU-8230. All these microscopes CFE-SEMs but only the latter provides the auto-flash system. Through this figure, twenty years of CFE microscopy is illustrated and one can clearly see the improvement that was achieved recently with the advent of the auto-flash CFE-SEM.

2.2 CFE-SEM for Low Voltage Microscopy

The main improvement in the design of new FE-SEMs, and particularly CFE-SEMs, resides in their ability to work routinely at very low voltages, i.e., lower than 1 kV, while keeping a small probe size at the nanometer scale. This is achieved through the use of a deceleration voltage applied at the specimen surface which decelerates the electron beam before it penetrates the sample. Combined to the high brightness and low chromatic aberration provided by the CFE technology, the spatial resolution thus obtained can be maintained close to the nanometer for voltages down to 30–50 V. The subtle gain of spatial resolution due to the auto-flash system can be observed in Fig. 2.3 where an alumina sphere was imaged in deceleration mode with a landing voltage of 0.7 kV without (SU-8000, Fig. 2.3a) and with the auto-flash (SU-8230, Fig. 2.3b) system. The same in-lens (top) detector was used in both images. Visually, the image obtained with the auto-flash option looks sharper with more details being observed compared to the image without it. The spatial resolution was measured via the SMART-J plugin based on the SMART program written by Joy (2002). The resulting resolution values were 2.5 and 2.0 nm for Fig. 2.3a, b, respectively, which represent an improvement of 20%.

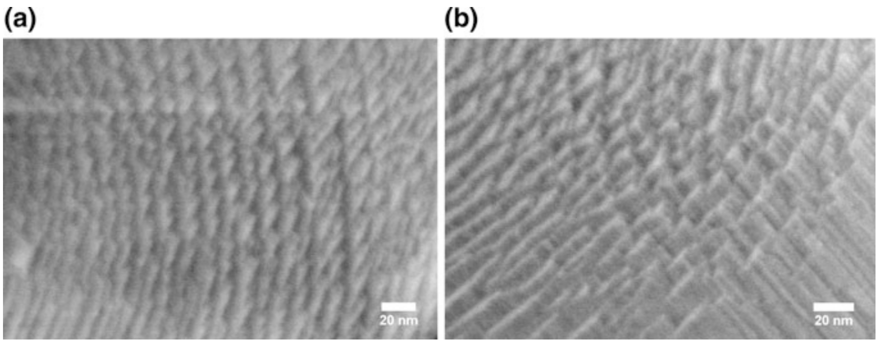

Fig. 2.3 Effect of the auto-flash system combined with vacuum improvement in the gun chamber through the comparison of alumina spheres at low accelerating voltage, E_L = 0.7 kV. **a** SU-8000 (E_0 = 2.5 kV, E_{dec} = 1.8 kV) in normal mode of operation, **b** SU-8230 (E_0 = 4.2 kV, E_{dec} = 3.5 kV) with the auto-flash system. A spatial resolution of 2.5 and 2.0 nm were measured with the SMART-J plugin for (**a**) and (**b**), respectively

The reduction of the primary electrons voltage has several advantages: First, through the reduction of the electron penetration range, a smaller volume contributes to the emitted signals, especially the BSEs and, as a consequence, the SE_2 (Joy 1985; Reimer 1998). Therefore, either SEs (SE_1 and SE_2) or BSEs signals benefits from a smaller depth of emission and the prime surface of the specimen can be analyzed down to a few surface layers at ultra-low voltage (El-Gomati and Wells 2001; Frank and Mullerova 2006; Mikmekova et al. 2007, 2013, 2015) making the FE-SEMs useful for surface analysis by imaging treated surfaces with the versatility of the SEM. The reduction of the penetration depth is depicted in Fig. 2.4a where the electron range was simulated based on Monte Carlo modeling using the Casino 2.42 program (Drouin et al. 2007). A thousand trajectories were simulated and

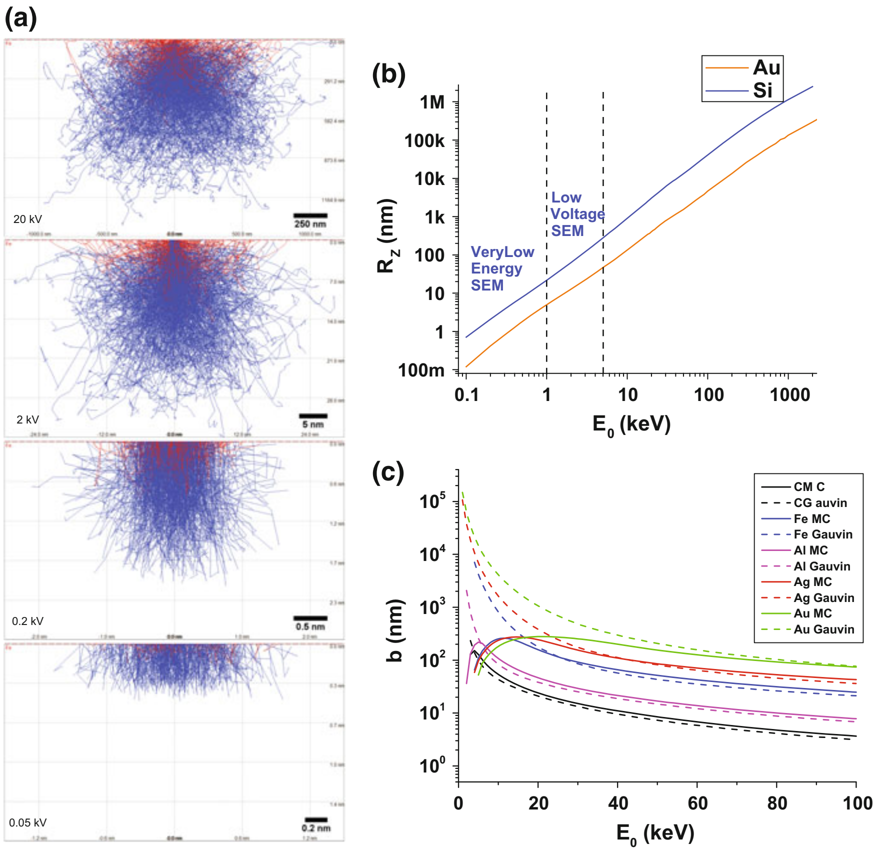

Fig. 2.4 **a** Effect of reducing the accelerating voltage on the electron diffusion volume, **b** range of voltages used in high resolution SEMs and **c** electron beam broadening *b* as a function of the accelerating voltage (E_0) for thin foils of 80 nm for C, Al, Fe, Ag, Au. The results obtained by calculations using the equation from Gauvin (Gauvin and Rudinsky 2016) (dashed lines) in (**c**) were compared with those obtained using Monte Carlo simulations (full lines)

displayed with accelerating voltages of 20, 2, 0.2, and 0.05 kV in a Fe target and the BSEs trajectories are displayed as the red lines. As can be noticed, the BSE range falls approximately from 300 nm at $E_0 = 20$ kV to 10, 1, and 0.2 nm for $E_0 =$ 2, 0.2, and 0.05 kV, respectively. A plot of the total electron range R_z as a function of the accelerating voltage for Si and Au is presented in Fig. 2.4b.

These curves clearly show the proportional log/log relationship of the two quantities, regardless of the atomic number for which the range is proportional to the atomic number Z as $Z^{-8/9}$ according to Kanaya and Okayama (1972). Secondly, the tilt dependence of the SE emission decreases (Cazaux 2005; Reimer 1993) with the accelerating voltage as shown in Fig. 2.5 providing a more uniform image contrast where the edge effect is highly diminished. Combined to these two important image-forming effects, the reduction of the beam voltage is also of great advantage regarding the damage inflicted to the specimen by the electron irradiation. The reduction of the beam voltage reduces greatly the temperature rise, which is proportional to the beam voltage, as well as the radiolysis that is reduced when the ionization energy is small in the irradiated volume. Especially for organic specimens, low voltage prevents from breaking the molecular groups, which is the main damage process observed for these materials (Reimer 1998). Finally, in some cases, the reduction of the accelerating voltage may be accompanied with a reduction of the charge effects. This is mostly applicable to several polymers as they have smaller E_2 voltages compared to ceramics and minerals (Joy et al. 1998; Joy and Joy 1996). However, this must be taken with precautions because, when the beam electron density is of the same order as that at higher voltage, the energy loss is concentrated in a dramatically smaller volume (see Fig. 2.4a) and thus can degrade the fragile charge balance of nonconductive materials.

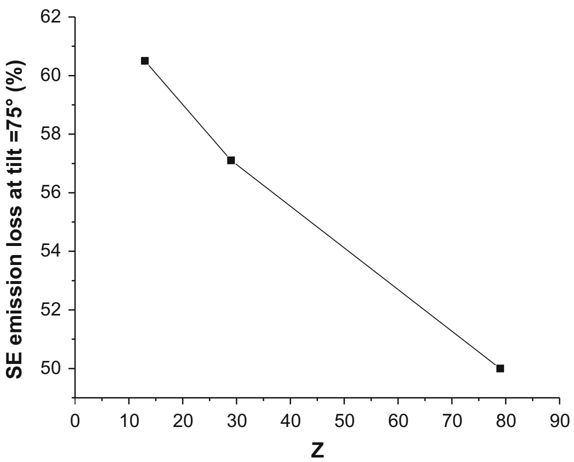

Fig. 2.5 Secondary electrons emission loss at a tilt angle of 75° for Al, Cu and Au when the accelerating voltage (E_0) is lowered from $E_0 = 10$ kV to $E_0 = 0.5$ kV. Data extracted from Reimer (Reimer 1993)

2.3 Scanning Transmission Microscopy in the SEM

Scanning transmission electron microscopy has revealed as an invaluable technique since the seventies to characterize material science specimens in the TEM (Crewe and Wall 1970; Crewe et al. 1968; Pennycook 1989; Pennycook et al. 1996). However, the use of high accelerating voltages in such microscopes is highly detrimental to the specimen stability, especially for low Z materials such as lithium or carbon (Egerton 2012; Egerton et al. 2004). In this regard, decreasing the beam voltage is becoming an increasing ground of research for the TEM/STEM community (Bendayan and Paransky 2014; Drummy 2014, Kaiser et al. 2011; Sasaki et al. 2010, 2014). Especially, due to the small chromatic aberration coefficient provided by CFE guns, high resolution CFE-SEMs and monochromator-fitted FE-SEMs nowadays provide the stability and the probe dimensions necessary to apply efficiently low voltage STEM in the SEM. In addition, SEM is an effective cost reduction compared to TEM/STEMs and their ease of use make them one of the most used technique for materials characterization around the world. Typically, a few minutes are generally necessary to achieve the highest image quality in STEM mode and this permits to provide high throughput for characterization laboratories. One interesting advantage of performing STEM in a SEM is its capability to work at low voltages with high stability, which is generally difficult to achieve with the high voltage-designed electron columns of TEM/STEMs. Therefore, the gain in contrast due to the increased interactions of low voltage electrons with the specimen can be optimized for a wide range of materials, especially low Z materials. This, combined with the limited beam broadening for voltages of 20–30 kV (Fig. 2.4c), makes the new generation of FE-SEMs ideal candidates for low voltage STEM and recently, atomic resolution has been reported with a CFE-SEM (Konno et al. 2014; Orai et al. 2014; Sunaoshi et al. 2012).

References

Bendayan, M., & Paransky, E. (2014). Perspectives on low voltage transmission electron microscopy as applied to cell biology. *Microscopy Research and Technique, 77,* 999–1004.

Cazaux, J. (2005). Recent developments and new strategies in scanning electron microscopy. *Journal of Microscopy, 217,* 16–35.

Crewe, A., & Wall, J. (1970). A scanning microscope with 5 nm resolution. *Journal of Molecular Biology, 48,* 375–393.

Crewe, A., Wall, J., & Welter, L. (1968). A high-resolution scanning transmission electron microscope. *Journal of Applied Physics, 39,* 5861–5868.

Drouin, D., Couture, A. R., Joly, D., Tastet, X., Aimez, V., & Gauvin, R. (2007). CASINO V2. 42—A fast and easy-to-use modeling tool for scanning electron microscopy and microanalysis users. *Scanning, 29*, 92–101.

Drummy, L. F. (2014). Electron microscopy of organic–inorganic interfaces: Advantages of low voltage. *Ultramicroscopy, 145,* 74–79.

Egerton, R. (2012). Mechanisms of radiation damage in beam-sensitive specimens, for TEM accelerating voltages between 10 and 300 kV. *Microscopy Research and Technique, 75,* 1550–1556.

Egerton, R., Li, P., & Malac, M. (2004). Radiation damage in the TEM and SEM. *Micron, 35,* 399–409.

El-Gomati, M., & Wells, T. (2001). Very-low-energy electron microscopy of doped semiconductors. *Applied Physics Letters, 79,* 2931.

Frank, L., & Mullerova, I. (2006). The scanning low energy electron microscopy (SLEEM) mode in SEM. *Microscopy and Microanalysis, 12,* 152–153.

Gauvin, R., & Rudinsky, S. (2016). A universal equation for computing the beam broadening of incident electrons in thin films. *Ultramicroscopy, 167,* 21–30.

Houdellier, F., de Knoop, L., Gatel, C., Masseboeuf, A., Mamishin, S., Taniguchi, Y., et al. (2015). Development of TEM and SEM high brightness electron guns using cold-field emission from a carbon nanotip. *Ultramicroscopy, 151*, 107–115.

Joy, D. (2002). SMART—A program to measure SEM resolution and imaging performance. *Journal of Microscopy, 208,* 24–34.

Joy, D. C. (1985). Resolution in low voltage scanning electron microscopy. *Journal of Microscopy, 140,* 283–292.

Joy, D. C., & Joy, C. S. (1996). Low voltage scanning electron microscopy. *Micron, 27,* 247–263.

Joy, D. C., Joy, C. S., et al. (1998). Study of the dependence of E2 energies on sample chemistry. *Microscopy and Microanalysis, 4*, 475–480.

Kaiser, U., Biskupek, J., Meyer, J., Leschner, J., Lechner, L., Rose, H., et al. (2011). Transmission electron microscopy at 20 kV for imaging and spectroscopy. *Ultramicroscopy, 111*, 1239–1246.

Kanaya, K., & Okayama, S. (1972). Penetration and energy-loss theory of electrons in solid targets. *Journal of Physics D: Applied Physics, 5,* 43.

Kasuya, K., Kawasaki, T., Moriya, N., Arai, M., & Furutsu, T. (2014). Magnetic field superimposed cold field emission gun under extreme-high vacuum. *Journal of Vacuum Science & Technology B, 32*, 031802.

Konno, M., Ogashiwa, T., Sunaoshi, T., Orai, Y., & Sato, M. (2014). Lattice imaging at an accelerating voltage of 30 kV using an in-lens type cold field-emission scanning electron microscope. *Ultramicroscopy, 145,* 28–35.

Mikmekova, S., Yamada, K., & Noro, H. (2013). TRIP steel microstructure visualized by slow and very slow electrons. *Microscopy, 62*(6), 589–596.

Mikmekova, S., Yamada, K., & Noro, H. (2015). Dual-phase steel structure visualized by extremely slow electrons. *Microscopy, 64*(6), 437–443.

Mullerova, I., Matsuda, K., Hrncirik, P., & Frank, L. (2007). Enhancement of SEM to scanning LEEM. *Surface Science, 601,* 4768–4773.

Orai, Y., Sunaoshi, T., Okada, S., Ogashiwa, T., Ito, H., & Konno, M. (2014). Application of low energy STEM with the in-lens cold FE-SEM. *Journal of Physics: Conference Series.*

Pennycook, S. (1989). Z-contrast STEM for materials science. *Ultramicroscopy, 30,* 58–69.

Pennycook, S., Jesson, D., McGibbon, A., & Nellist, P. (1996). High angle dark field STEM for advanced materials. *Journal of Electron Microscopy, 45,* 36–43.

Reimer, L. (1993). *Image formation in low-voltage scanning electron microscopy (SPIE tutorial text Vol. TT12) (Tutorial texts in optical engineering),* USA: SPIE Press.

Reimer, L. (1998). *Scanning electron microscopy: Physics of image formation and microanalysis (Springer series in optical sciences)*. Berlin: Springer.

Sasaki, T., Sawada, H., Hosokawa, F., Kohno, Y., Tomita, T., Kaneyama, T., et al. (2010). Performance of low-voltage STEM/TEM with delta corrector and cold field emission gun. *Journal of Electron Microscopy, 59,* S7–S13.

Sasaki, T., Sawada, H., Hosokawa, F., Sato, Y., & Suenaga, K. (2014). Aberration-corrected STEM/TEM imaging at 15kV. *Ultramicroscopy, 145,* 50–55.

Sunaoshi, T., Orai, Y., Ito, H., Ogashiwa, T., Agemura, T., & Konno, M. (2012). 30 kV stem imaging with lattice resolution using a high resolution cold FE-SEM. In: *Proceedings of the 15th European Microscopy Congress,* Manchester Central, United Kingdom, September 16–21.

Springer
http://www.springer.com/978-981-10-4432-8

Field Emission Scanning Electron Microscopy
New Perspectives for Materials Characterization
Brodusch, N.; Demers, H.; Gauvin, R.
2018, XII, 137 p. 53 illus., 20 illus. in color., Softcover
ISBN: 978-981-10-4432-8